nature physics

LETTERS

PUBLISHED ONLINE: 9 MARCH 2014 | DOI: 10.1038/NPHYS2887

Topological excitations and the dynamic structure factor of spin liquids on the kagome lattice

Matthias Punk[1,2], Debanjan Chowdhury[1] and Subir Sachdev[1]*

Recent neutron scattering experiments on the spin-1/2 kagome lattice antiferromagnet $ZnCu_3(OH)_6Cl_2$ (Herbertsmithite) provide the first evidence of fractionalized excitations in a quantum spin liquid state in two spatial dimensions[1]. In contrast to existing theoretical models of both gapped and gapless spin liquids[2–8], which give rise to sharp dispersing features in the dynamic structure factor[9,10], the measured dynamic structure factor reveals an excitation continuum that is remarkably flat as a function of frequency. Here we show that many experimentally observed features can be explained by the presence of topological vison excitations in a Z_2 spin liquid[11]. These visons form flat bands on the kagome lattice, and thus act as a momentum sink for spin-carrying excitations that are probed by neutron scattering. We compute the dynamic structure factor for two different Z_2 spin liquids[2] and find that our results for one of them are in qualitative agreement with the neutron scattering experiments above a very low energy cutoff, below which the structure factor is probably dominated by impurities.

Herbertsmithite, a layered spin-1/2 kagome lattice antiferromagnet[12], is one of the strongest contenders for an experimental realization of a spin liquid state[13]. Indeed, no sign of magnetic ordering is observed down to temperatures around 50 mK, whereas the natural energy scale set by the magnetic exchange coupling $J \sim 200$ K is four orders of magnitude larger[14]. Neutron scattering experiments[1] on single crystals of this material are consistent with a continuum of fractionalized spinon excitations as expected in a quantum spin liquid state. However, mean-field theories predict a vanishing structure factor below the onset of the two-spinon continuum, which is at a finite energy even for gapless spin liquids, apart from the small set of crystal momenta where the spinon gap closes. This is in stark contrast to experiments, where the measured structure factor is finite and almost constant as a function of frequency down to energies of the order of $\sim J/10$ (ref. 1).

Here we propose an explanation for the lack of a momentum-dependent spinon continuum threshold via the interaction of spinons with another set of excitations which form a (nearly) flat band. Such localized excitations act as a momentum sink for the spinons, thereby flattening the dynamic structure factor. So far, the only theoretical model for a spin liquid state on the kagome lattice which naturally gives rise to a flat excitation band at low energies consists of the Z_2 spin liquids[2–4]. Besides spinons, these states exhibit gapped vortex excitations[15,16] of an emergent Z_2 gauge field[17,18], so-called visons[11], which indeed have a lowest energy band that is nearly flat[19,20]. Because the visons carry neither charge nor spin, they do not couple directly to neutrons. They interact with spinons, however, and we show that this coupling is responsible for flattening the dynamic structure factor and removing the sharp onset at the two-spinon continuum, in accordance with experimental results. Note that the vison gap has to be small for this mechanism to work. This assumption is justified by numerical density matrix renormalization group calculations[21–23], which indicate that a Z_2 spin liquid ground-state on the kagome lattice is proximate to a valence bond solid (VBS) transition, at which the vison gap vanishes.

Model

Our aim is to compute the dynamic structure factor for two Z_2 spin liquids that have been discussed in detail in ref. 2. We start from the standard bosonic spin liquid mean-field theory of the spin-1/2 antiferromagnetic Heisenberg model on the kagome lattice. Using a Schwinger-boson representation of the spin-1/2 operators $\mathbf{S}_i = b^\dagger_{i\alpha}\boldsymbol{\sigma}_{\alpha\beta}b_{i\beta}/2$, where $\boldsymbol{\sigma}$ denotes the vector of Pauli matrices and $b^\dagger_{i\alpha}$ is the creation operator of a boson with spin α on lattice site i, and performing a mean-field decoupling in the spin-singlet channel, the Heisenberg Hamiltonian can be written as

$$H_b = -J\sum_{\langle i,j\rangle} Q^*_{ij}\,\varepsilon_{\alpha\beta}\,b_{i\alpha}b_{j\beta} + \text{h.c.} + \lambda\sum_i b^\dagger_{i\alpha}b_{i\alpha}$$

with $Q^*_{ij} = \langle \varepsilon_{\alpha\beta}\, b^\dagger_{i\alpha}b^\dagger_{j\beta}\rangle/2$, $\varepsilon_{\alpha\beta}$ is the fully antisymmetric tensor of SU(2), h.c. is the hermitian conjugate term and λ denotes the Lagrange multiplier that fixes the constraint of one Schwinger boson per lattice site. Sums over Greek indices are implicit. To study the effect of vison excitations on the spinons, we have to include phase fluctuations of the mean-field variables Q_{ij} in our theory. The Z_2 spin liquid corresponds to the Higgs phase of the resulting emergent gauge theory, where the phase fluctuations are described by an Ising bond variable σ^z_{ij}. The Hamiltonian describing bosonic spinons and their coupling to the Ising gauge field takes the form

$$\begin{aligned} H \;=\; & -J\sum_{\langle i,j\rangle}\sigma^z_{ij}\left(Q^*_{ij}\,\varepsilon_{\alpha\beta}\,b_{i\alpha}b_{j\beta} + \text{h.c.}\right) + \lambda\sum_i b^\dagger_{i\alpha}b_{i\alpha} \\ & + K\sum_{\text{plaq.}}\prod_{\text{plaq.}}\sigma^z_{ij} - h\sum_{\langle i,j\rangle}\sigma^x_{ij} \end{aligned} \qquad (1)$$

where the terms on the second line are responsible for the dynamics of the gauge field σ^z_{ij}. K and h are phenomenological parameters that set the energy scale for fluctuations of the Z_2 gauge field. Vison excitations are vortices of this emergent Z_2 gauge field—that is, excitations where the product $\prod\sigma^z_{ij}$ on a plaquette changes sign. For practical calculations it is more convenient to switch to a dual description of the Z_2 gauge field in terms of its vortex excitations[24], where the pure gauge field terms in the second line of equation (1) take the form of a fully-frustrated Ising model on the dice lattice. This model has been studied in detail in refs 19 and 20 and gives rise to three flat vison bands if restricted to nearest-neighbour vison

[1]Department of Physics, Harvard University, Cambridge, Massachussetts 02138, USA. [2]Institute for Theoretical Physics, University of Innsbruck, 6020 Innsbruck, Austria. *e-mail: sachdev@g.harvard.edu

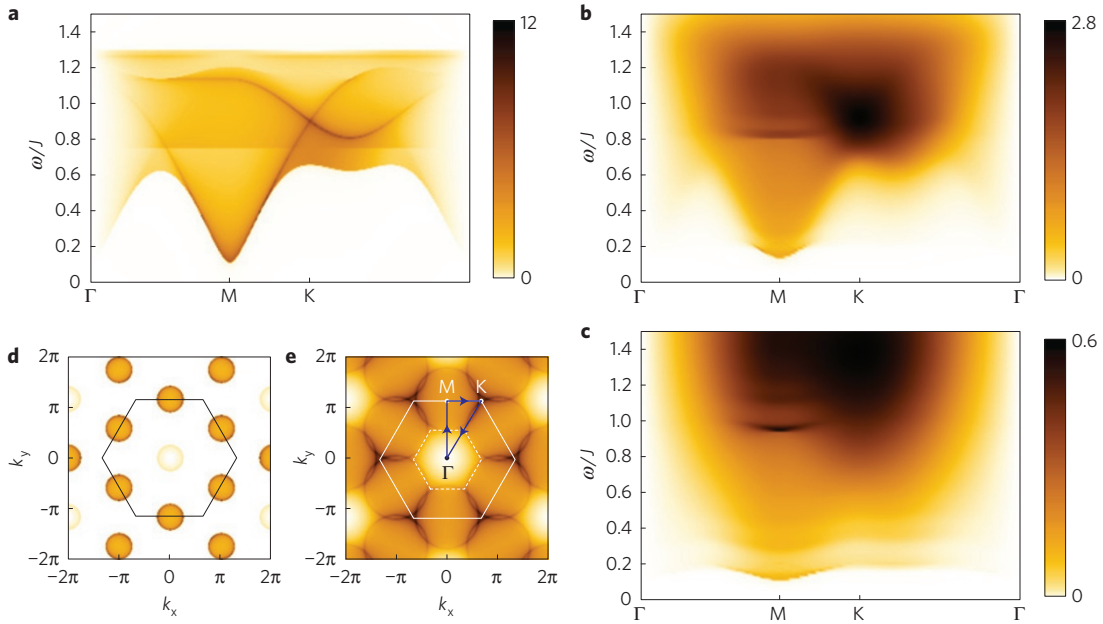

Figure 1 | Density plots of the the dynamic spin-structure factor $S(\mathbf{k},\omega)$ for the $Q_1 = Q_2$ spin liquid state. a–c, Plots of $S(\mathbf{k},\omega)$ at zero temperature for different spinon–vison interaction strengths as a function of frequency and momentum along the high-symmetry directions between the Γ, M and K points of the extended Brillouin zone, indicated by the blue arrows in **e**. **a**, Non-interacting spinons. Note that in the $Q_1 = Q_2$ state two of the three spinon bands are degenerate, whereas the third, highest energy spinon band is flat. This flat spinon band gives rise to the horizontal feature at $\omega \simeq 0.75J$. **b**, Spinon–vison interaction $g_0 = 0.2$. **c**, Spinon–vison interaction $g_0 = 0.6$. **d**,**e**, $S(\mathbf{k},\omega)$ for non-interacting spinons at fixed frequency $\omega/J = 0.4$ (**d**) and $\omega/J = 0.85$ (**e**). The elementary Brillouin zone of the kagome lattice is indicated by a dashed hexagon in **e**. Note the sharp onset of the two-spinon continuum for non-interacting spinons in **a** and **d**, which is washed out when interactions with visons are accounted for. All data in this figure were calculated for $|Q_1| = 0.4$ and the spinon gap was fixed at $\Delta_s \simeq 0.05J$. The vison gap is set to $\Delta_v = 0.025J$ in **b** and **c**.

hopping. As only the gap to the lowest vison band is small, we neglect the effects of the other two bands in the following.

The coupling between spinons and visons is a long-range statistical interaction (a spinon picks up a Berry's phase of π when encircling a vison[20]), which cannot be expressed in the form of a simple local Hamiltonian in the vortex representation. However, the fact that visons on the dice lattice are non-dispersing comes to the rescue here. Because these excitations are localized and can only be created in pairs, the long-range statistical interaction is effectively cancelled. Indeed, if a spinon is carried around a pair of visons, it does not pick up a Berry's phase. This is in precise analogy to an electron carried around a pair of superconducting Abrikosov vortices, where the total encircled flux is 2π and thus no phase is accumulated. The vison pairs are excited locally by a spinon, and thus it is reasonable to model the spinon–vison interaction by a local energy–energy coupling, neglecting the long-range statistical part. Accordingly we choose the simplest, gauge-invariant Hamiltonian of bosonic spinons on the kagome lattice coupled to a single, non-dispersing vison mode on the dual Dice lattice

$$\begin{aligned} H &= H_b + \sum_i \Delta_v \phi_i \phi_i \\ &\quad + g_0 \Delta_v \sum_{\substack{i \in \mathrm{Dice}_3 \\ \ell, m \in \nabla_i}} \phi_i \phi_i \left(\varepsilon_{\alpha\beta} Q^*_{\ell m} b_{\ell\alpha} b_{m\beta} + \mathrm{h.c.} \right) \end{aligned} \qquad (2)$$

Here, the real field ϕ_i describes visons living on the dice lattice sites i, g_0 denotes the spinon–vison coupling strength and Δ_v is the vison gap. The sum in the interaction term runs only over the three-coordinated Dice lattice sites i and couples the spinon bond energy on the triangular kagome plaquettes to the local vison gap at the plaquette centre. Further terms, where spinons on the hexagonal kagome plaquettes interact with visons at the centre of the hexagons are allowed, but neglected for simplicity.

A more detailed discussion of this interaction term can be found in the Supplementary Methods. We are going to compute the dynamic structure factor $S(\mathbf{k},\omega)$ using the model equation (2) for a particular Z_2 spin liquid state that has been identified in ref. 2. For the nearest-neighbour kagome antiferromagnet there are two independent bond expectation values $Q_{ij} \in \{Q_1, Q_2\}$ and the two distinct, locally stable mean-field solutions have $Q_1 = Q_2$ or $Q_1 = -Q_2$. The $Q_1 = Q_2$ state has flux π in the elementary hexagons, whereas the $Q_1 = -Q_2$ state is a zero-flux state. During the remainder of this article we focus only on the $Q_1 = Q_2$ state, as it gives rise to a little peak in $S(\mathbf{k},\omega)$ at small frequencies at the M point of the extended Brillouin zone, in accordance with experimental results. Results for the other state are discussed in the Supplementary Methods. Two other bosonic Z_2 states have been identified on the kagome lattice[3], but we refrain from computing the structure factor for these states, because both have a doubled unit cell, which complicates the calculations considerably.

Dynamic structure factor

Neutron scattering experiments measure the dynamic structure factor

$$S(\mathbf{k},\omega) = \frac{1}{N} \sum_{i,j} \mathrm{e}^{i\mathbf{k}\cdot(\mathbf{R}_i - \mathbf{R}_j)} \int \mathrm{d}t\, \mathrm{e}^{-i\omega t} \langle \mathbf{S}_i(t) \cdot \mathbf{S}_j(0) \rangle$$

which we are going to compute for the model presented in equation (2). Here $\mathbf{R}_i$ denotes the position of lattice site i. Note that $S(\mathbf{k},\omega)$ is periodic in the extended Brillouin zone depicted in (Fig. 1e). After expressing $\mathbf{S}_i \cdot \mathbf{S}_j$ in terms of Schwinger bosons and diagonalizing the free spinon Hamiltonian with

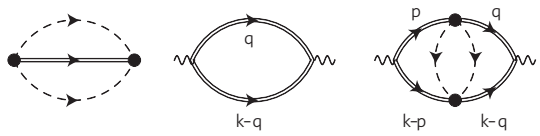

Figure 2 | Feynman diagrams for the spinon self energy and spin susceptibility for the theory in equation (2). Spinon self energy (left), one-loop contribution to the spin susceptibility (middle) and corresponding lowest order vertex correction (right). Double lines are dressed spinon propagators and dashed lines are bare vison propagators.

a Bogoliubov transformation, the one-loop expression for the dynamic spin susceptibility shown in Fig. 2, $\chi(\mathbf{k}, i\omega_n)$, can be derived straightforwardly (Methods). The dynamic structure factor can then be obtained from the susceptibility via

$$S(\mathbf{k},\omega) = \frac{\mathrm{Im}\,\chi(\mathbf{k}, i\omega_n \to \omega + i0^+)}{1 - \mathrm{e}^{-\beta\omega}}$$

Results of this calculation at zero temperature are shown in Figs 1 and 3 for the $Q_1 = Q_2$ state for different spinon–vison interaction strengths g_0. In the region around and between the high-symmetry points M and K the lowest order vertex correction shown in Fig. 2 gives only a relatively small contribution to $S(\mathbf{k},\omega)$ and thus has been neglected in the data shown in these figures (see Supplementary Methods for a discussion).

Discussion

Figure 1 shows the two-spinon contribution to the dynamic structure factor for the $Q_1 = Q_2$ state (results for the $Q_1 = -Q_2$ state can be found in the Supplementary Methods). The onset of the two-spinon continuum, which has a minimum at the M point, is clearly visible in Fig. 1a as the line of frequencies below which the dynamic structure factor vanishes. Moreover, several sharp peaks appear inside the spinon continuum. We note that such features in the two-spinon contribution to $S(\mathbf{k},\omega)$ are generic and are present also for gapless Dirac spin liquids.

Figure 1b,c show the dynamic structure factor along the same high-symmetry directions as in Fig. 1a, but now including the effect of spinon-induced vison pair production for two different interaction strengths g_0. The non-dispersing visons act as a powerful momentum sink for the spinons and lead to a considerable shift of spectral weight below the two-spinon continuum. The computed structure factor is considerably flattened at intermediate energies. Our results for the $Q_1 = Q_2$ state also capture the small low-frequency peak in $S(\mathbf{k},\omega)$ at the M point, which has been seen in experiment. This peak is a remnant of a minimum in the threshold of the two-spinon continuum at the M point, and we conjecture that it might be an indication that this particular Z_2 spin liquid state is realized in Herbertsmithite. In Fig. 3 we show plots of $S(\mathbf{k},\omega)$ at constant energy, where this peak is clearly visible, and compare our results qualitatively to the experimental data. Note that we did not choose the parameters to fit the experimental data, instead we tried to use reasonable values for the spinon gap $\Delta_s \simeq 0.05J$ and the vison gap $\Delta_v = 0.025J$ to make features related to the momentum-independent onset of the dynamic structure factor better visible. Also the spinon bandwith was adjusted to be on the order of J.

In Fig. 1c, 3g one can barely see small oscillations of $S(\mathbf{k},\omega)$ at low frequencies. These oscillations originate from the self-consistent computation of the spinon self-energy $\Sigma(\mathbf{k},\omega)$ and are related to resonances in the self-energy at energies corresponding to the creation of two, four and higher even numbers of vison excitations.

The experimental results show a strong increase of the dynamic structure factor at energies below 1meV away from the M point. We attribute this feature to impurity spins, which are not accounted for in our approach. In Herbertsmithite excess copper substitutes for zinc in the interlayer sites. These spin-1/2 impurities are only weakly coupled to the kagome layers, with an exchange constant that is on the order of one kelvin[25]. Although it is unlikely that these impurities contribute considerably to a flattening of the dynamical structure factor as discussed in this paper, we believe they are responsible for the above-mentioned low-energy contribution. This is in accordance with recent low-energy neutron scattering measurements on powder samples of Herbertsmithite[26], but a detailed calculation remains an open problem for future study. Also note that such a low-energy contribution would hide the momentum-independent onset of the dynamic structure factor, which is at the energy $\omega_{\mathrm{onset}} = 2\Delta_v + 2\Delta_s$ in the scenario discussed here.

Dzyaloshinskii–Moriya (DM) interactions as well as an easy-axis anisotropy on the order of $\sim J/10$ are known to exist in Herbertsmithite, but have been neglected in our analysis for simplicity. The effect of DM interactions has been studied within a $1/N$ expansion[9,27], where the $Q_1 = Q_2$ state is favoured over the $Q_1 = -Q_2$ state if the DM interactions are sufficiently strong.

Last, neutron scattering experiments explored energies up to $\omega \simeq 0.65J$ and concluded that the integrated weight accounts for roughly 20% of the total moment sum rule[1]. Consequently it is reasonable to expect that the dynamic structure factor is finite up to energies of a few J. For the parameters chosen in our calculation (that is $Q_1 = 0.4$ and a spinon gap $\Delta_s = 0.05$) the structure factor for non-interacting spinons has a sharp cutoff at an energy around $\omega \simeq 1.3J$, corresponding to roughly twice the spinon bandwidth. However, if interactions with visons are included, this upper cutoff is shifted to considerably larger energies. For a spinon–vison coupling $g_0 = 0.6$, the structure factor has a smooth upper cutoff at an energy around $\omega \simeq 3J$. Such large bandwidths are hardly achievable in theories with non-interacting spinons. We note that similarly large bandwidths have been found in exact diagonalization studies[28].

Methods

The one-loop expression for the dynamic spin susceptibility, $\chi(\mathbf{k}, i\omega_n)$, is given by

$$\begin{aligned}\chi(\mathbf{k}, i\omega_n) \quad = \quad & \frac{3}{2}\sum_{\mathbf{q},\Omega_n} G_\ell(\mathbf{q}, i\Omega_n) G_m(\mathbf{k}-\mathbf{q}, i\omega_n - i\Omega_n) \\ & \times \left[U_{j\ell}(\mathbf{q}) V_{jm}(\mathbf{k}-\mathbf{q}) + V_{j\ell}(\mathbf{q}) U_{jm}(\mathbf{k}-\mathbf{q})\right] \\ & \times U^*_{i\ell}(\mathbf{q}) V^*_{im}(\mathbf{k}-\mathbf{q}) + \ldots\end{aligned}$$

where the dots represent similar terms that give a contribution at negative frequencies after analytic continuation and thus play no role in calculating $S(\mathbf{k},\omega)$ at zero temperature. Note that we are working in a Matsubara representation here, where the spin-susceptibility $\chi(\mathbf{k}, i\omega_n)$ and the spinon propagator $G(\mathbf{q}, i\Omega_n)$ are expressed as functions of the bosonic Matsubara frequencies $i\Omega_n$ and $i\omega_n$. The summation over the sublattice indices $i,j,\ell,m \in \{1,2,3\}$ is implicit here and the 3×3 matrices U_{ij} and V_{ij} form the Bogoliubov rotation matrix

$$M = \begin{pmatrix} U & -V^* \\ V & U^* \end{pmatrix}$$

as defined in ref. 2, which diagonalizes the mean-field spinon Hamiltonian. $G_\ell(\mathbf{q}, i\Omega_n)$ denotes the dressed spinon Green's function with band-index ℓ

$$G^{-1}_\ell(\mathbf{q}, i\Omega_n) = i\Omega_n - \epsilon_\ell(\mathbf{q}) - \Sigma_\ell(\mathbf{q}, i\Omega_n)$$

where $\epsilon_\ell(\mathbf{q})$ is the bare spinon dispersion. The spinon self-energy (Fig. 2), which we compute self-consistently, is determined by the equation

$$\Sigma_\ell(\mathbf{q}, i\Omega_n) = \sum_{\mathbf{p},m} \lambda^\dagger_{\ell m}(\mathbf{p},\mathbf{q}) \lambda_{m\ell}(\mathbf{p},\mathbf{q}) G_m(i\Omega_n - 2\Delta_v, \mathbf{p})$$

Here the 6×6 matrix $\lambda(\mathbf{p},\mathbf{q})$ denotes the bare spinon–vison interaction vertex, with $\mathbf{p}$ ($\mathbf{q}$) the momentum of the outgoing (incoming) spinon. Note that the six

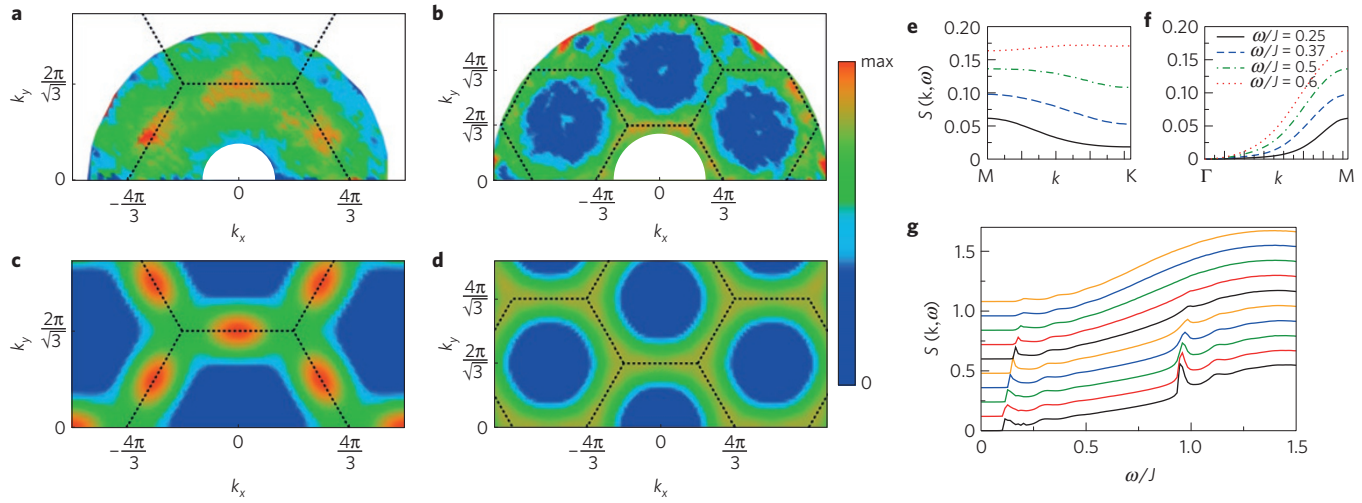

Figure 3 | Qualitative comparison between experimental measurements[1] and our theoretical results for the dynamic structure factor $S(\mathbf{k},\omega)$. **a**,**b**, Experimental data at fixed frequency are shown for $\omega = 0.75$ meV (**a**) and $\omega = 6$ meV (**b**). **c**,**d**, Theoretical results for the $Q_1 = Q_2$ spin liquid at fixed frequency are plotted for $\omega = 0.37J$ (**c**) and $\omega = 0.6J$ (**d**). The extended Brillouin zone is indicated by the dashed hexagons. Note that the peak at the M point at low frequencies, as well as the flatness of $S(\mathbf{k}, \omega)$ between the M and K points at higher frequencies is captured by our theory. **e**,**f**, Cuts of our theoretical results for $S(\mathbf{k}, \omega)$ along high-symmetry directions at different frequencies are plotted between the M and K point (**e**), as well as between the Γ and M point (**f**), again showing the peak at the M point at low frequencies. **g**, Details of the calculated structure factor as a function of frequency for various momenta between the M (bottom curve) and K point (top curve). Note that all curves in **g** are shifted by 0.12 J with respect to each other for better visibility. All theoretical data shown was computed for the $Q_1 = Q_2$ state with a spinon–vison interaction strength $g_0 = 0.6$ and other parameters as in Fig. 1.

spinon bands come in three degenerate pairs owing to the SU(2) spin-symmetry. Furthermore, note that the flat vison band is not renormalized at arbitrary order in the spinon–vison coupling.

We emphasize here that a self-consistent computation of the spinon self-energy is necessary, because the real part of $\Sigma(\mathbf{k},\omega)$ is large and broadens the spinon bands. A non-self-consistent computation thus leads to sharp spinon excitations above the bare spinon band, which are unphysical as they would decay immediately via vison pair production. A different approximation, which circumvents this problem, would be to calculate $\Sigma(\mathbf{k},\omega)$ non-self-consistently and neglect the real part completely. This approximation violates sum rules however, as the integrated spectral weight of the spinon is no longer unity (for a detailed discussion, see the Supplementary Methods).

Note that we do not determine the parameters $|Q_1|$ and λ variationally. Instead, we use them to fix the spinon gap as well as the spinon bandwidth. $|Q_1|$ is restricted to values between 0 and $1/\sqrt{2}$ and quantifies antiferromagnetic correlations of nearest-neighbour spins ($|Q_1| = 1/\sqrt{2}$ if nearest-neighbour spins form a singlet). All data shown in this paper was computed for $|Q_1| = 0.4$, and λ has been adjusted such that the spinon gap takes the value $\Delta_s/J \simeq 0.05$. As mentioned in the introduction, we assume that the vison gap Δ_v is small owing to evidence of proximity to a VBS state, and we chose $\Delta_v/J = 0.025$ for all data shown in this Article—namely, the vison gap is roughly half the spinon gap.

Received 23 August 2013; accepted 10 January 2014; published online 9 March 2014; corrected after print 22 April 2016

References

1. Han, T-H. *et al.* Fractionalized excitations in the spin-liquid state of a kagome-lattice antiferromagnet. *Nature* **492,** 406–410 (2012).
2. Sachdev, S. Kagome- and triangular-lattice Heisenberg antiferromagnets: Ordering from quantum fluctuations and quantum-disordered ground states with unconfined bosonic spinons. *Phys. Rev. B* **45,** 12377 (1992).
3. Wang, F. & Vishwanath, A. Spin-liquid states on the triangular and Kagome lattices: A projective-symmetry-group analysis of Schwinger boson states. *Phys. Rev. B* **74,** 174423 (2006).
4. Lu, Y-M., Ran, Y. & Lee, P. A. Z_2 spin liquids in the $S = 1/2$ Heisenberg model on the kagome lattice: A projective symmetry-group study of Schwinger fermion mean-field states. *Phys. Rev. B* **83,** 224413 (2011).
5. Iqbal, Y., Becca, F. & Poilblanc, D. Projected wave function study of Z_2 spin liquids on the kagome lattice for the spin-1/2 quantum Heisenberg antiferromagnet. *Phys. Rev. B* **84,** 020407 (2011).
6. Tay, T. & Motrunich, O. I. Variational study of $J_1 - J_2$ Heisenberg model on kagome lattice using projected Schwinger-boson wave functions. *Phys. Rev. B* **84,** 020404(R) (2011).
7. Tay, T. & Motrunich, O. I. Sign structures for short-range RVB states on small kagome clusters. *Phys. Rev. B* **84,** 193102 (2011).
8. Hao, Z. & Tchernyshyov, O. Spin-1/2 Heisenberg antiferromagnet on the kagome lattice: Z_2 spin liquid with fermionic spinons. *Phys. Rev. B* **87,** 214404 (2013).
9. Messio, L., Cepas, O. & Lhullier, C. Schwinger-boson approach to the kagome antiferromagnet with Dzyaloshinskii–Moriya interactions: Phase diagram and dynamical structure factors. *Phys. Rev. B* **81,** 064428 (2010).
10. Dodds, T., Bhattacharjee, S. & Kim, Y. B. Quantum spin liquids in the absence of spin-rotation symmetry: Application to Herbertsmithite. *Phys. Rev. B* **88,** 224413 (2013).
11. Senthil, T. & Fisher, M. P. A. Z_2 gauge theory of electron fractionalization in strongly correlated systems. *Phys. Rev. B* **62,** 7850–7881 (2000).
12. Shores, M. P., Nytko, E. A., Bartlett, B. M. & Nocera, D. G. A structurally perfect $s = 1/2$ kagome antiferromagnet. *J. Am. Chem. Soc.* **127,** 13462–13463 (2005).
13. De Vries, M. A. *et al.* Scale-free antiferromagnetic fluctuations in the $s = 1/2$ kagome antiferromagnet herbertsmithite. *Phys. Rev. Lett.* **103,** 237201 (2009).
14. Helton, J. S. *et al.* Spin dynamics of the spin−1/2 kagome lattice antiferromagnet $ZnCu_3(OH)_6Cl_2$. *Phys. Rev. Lett.* **98,** 107204 (2007).
15. Read, N. & Chakraborty, B. Statistics of the excitations of the resonating-valence-bond state. *Phys. Rev. B* **40,** 7133–7140 (1989).
16. Kivelson, S. Statistics of holons in the quantum hard-core dimer gas. *Phys. Rev. B* **39,** 259–264 (1989).
17. Read, N. & Sachdev, S. Large-N expansion for frustrated quantum antiferromagnets. *Phys. Rev. Lett.* **66,** 1773–1776 (1991).
18. Wen, X-G. Mean-field theory of spin-liquid states with finite energy gap and topological orders. *Phys. Rev. B* **44,** 2664–2672 (1991).
19. Nikolic, P. & Senthil, T. Physics of low-energy singlet states of the kagome lattice quantum Heisenberg antiferromagnet. *Phys. Rev. B* **68,** 214415 (2003).
20. Huh, Y., Punk, M. & Sachdev, S. Vison states and confinement transitions of Z_2 spin liquids on the kagome lattice. *Phys. Rev. B* **84,** 094419 (2011).
21. Yan, S., Huse, D. A. & White, S. R. Spin-liquid ground state of the $s = 1/2$ kagome Heisenberg antiferromagnet. *Science* **332,** 1173–1176 (2011).
22. Jiang, H. C., Wang, Z. & Balents, L. Identifying topological order by entanglement entropy. *Nature Phys.* **8,** 902–905 (2012).

23. Depenbrock, S., McCulloch, I. P. & Schollwöck, U. Nature of the spin-liquid ground state of the $s=1/2$ Heisenberg model on the kagome lattice. *Phys. Rev. Lett.* **109,** 067201 (2012).
24. Wegner, F. Duality in generalized Ising models and phase transitions without local order parameters. *J. Math. Phys.* **12,** 2259–2272 (1971).
25. Bert, F. *et al.* Low temperature magnetization of the $S=1/2$ kagome antiferromagnet $ZnCu_3(OH)_6Cl_2$. *Phys. Rev. B* **76,** 132411 (2007).
26. Nilsen, G. J., de Vries, M. A., Stewart, J. R., Harrison, A. & Ronnow, H. M. Low-energy spin dynamics of the $s=1/2$ kagome system herbertsmithite. *J. Phys. Condens. Matter* **25,** 106001 (2013).
27. Huh, Y., Fritz, L. & Sachdev, S. Quantum criticality of the kagome antiferromagnet with Dzyaloshinskii–Moriya interactions. *Phys. Rev. B* **81,** 144432 (2010).
28. Laeuchli, A. M. & Lhuillier, C. Dynamical correlations of the kagome $s=1/2$ Heisenberg quantum antiferromagnet. Preprint available at http://arxiv.org/0901.1065.

Acknowledgements

We acknowledge illuminating discussions with M. Babadi, S. Gopalakrishnan, M. Lawler, J. D. Sau and especially Y. S. Lee. Furthermore, we thank T-H. Han and Y. S. Lee for providing the neutron scattering data shown in Fig. 3. This research was supported by the US NSF under Grant DMR-1103860 and by the John Templeton Foundation. This research was also supported in part by the Perimeter Institute for Theoretical Physics; research at the Perimeter Institute is supported by the Government of Canada through Industry Canada and by the Province of Ontario through the Ministry of Research and Innovation. M.P. is supported by the Erwin Schrödinger Fellowship J 3077-N16 of the Austrian Science Fund (FWF). The computations were performed in part on the Odyssey cluster supported by the FAS Science Division Research Computing Group at Harvard University.

Author contributions

M.P. performed the numerical computations. M.P., D.C. and S.S. contributed to the theoretical research described in the paper and the writing of the manuscript.

Additional information

Supplementary information is available in the online version of the paper. Reprints and permissions information is available online at www.nature.com/reprints. Correspondence and requests for materials should be addressed to S.S.

Competing financial interests

The authors declare no competing financial interests.

Erratum: Topological excitations and the dynamic structure factor of spin liquids on the kagome lattice

Matthias Punk, Debanjan Chowdhury and Subir Sachdev

Nature Physics **10,** 289–293 (2014); published online 9 March 2014; corrected after print 22 April 2016.

In the version of this Letter originally published square root symbols were mistakenly included in the *x*-axis tick labels in Figure 3a–d. This has now been corrected in the online versions of the Letter.

Figure 3